Water Resources Management **18:** 177–199, 2004.

High-resolution Numerical Simulation of Flow Through a Highly Sinuous River Reach

JOSÉ F. RODRIGUEZ[1*], FABIÁN A. BOMBARDELLI[2], MARCELO H. GARCÍA[3], KELLY M. FROTHINGHAM[4], BRUCE L. RHOADS[5] and JORGE D. ABAD[3]

[1] *School of Engineering, The University of Newcastle, Callaghan, New South Wales, Australia;* [2] *Department of Civil and Environmental Engineering, University of California at Davis, Davis, California, U.S.A.;* [3] *Van Te Chow Hydrosystems Laboratory, Department of Civil and Environmental Engineering, University of Illinois at Urbana-Champaign, Urbana, Illinois, U.S.A.;* [4] *Department of Geography and Planning, Buffalo State College, Buffalo, New York, U.S.A.;* [5] *Department of Geography, University of Illinois at Urbana-Champaign, Urbana, Illinois, U.S.A.*
(author for correspondence, e-mail: jose.rodriguez@newcastle.edu.au)*

(Received: 31 May 2001; in final form: 4 November 2003)

Abstract. River dynamics involve complex, incompletely understood interactions among flow, sediment transport and channel form. The capacity to predict these interactions is essential for a variety of river management problems, including channel migration, width adjustment and habitat development. To address this need, high-resolution numerical models increasingly are being used by river engineers, fluvial geomorphologists and river biologists to explore the complexity of river dynamics and to predict fluvial behavior. This paper presents numerical simulations through a natural meandering river using two different models: a depth-averaged numerical code with secondary flow correction and a fully 3-D, state-of-the-art, Computational-Fluid-Dynamics (CFD) code. Models predictions are compared to high-quality 3-D velocity data collected in a highly sinuous reach of the Embarras River in Central Illinois, showing a successful simulation of the main flow features. Implications for sediment transport, planform development and habitat structure throughout the reach are analyzed, demonstrating the potential use of the models as a tool for river management.

Key words: Acoustic Doppler Velocimeter, computational fluid dynamics, depth-averaged modeling, meandering rivers, meanders, secondary circulation

1. Introduction

The growing concern about environmental management of river systems has led to an increasing reliance on numerical simulations to support prediction, design and decision-making. The traditional focus on a single management objective, such as flood-control or navigation, is being replaced by multi-objective management that emphasizes the importance of environmental quality and the need to evaluate interrelations among hydraulic, geomorphological and ecological components of river systems over a range of spatial and temporal scales (Frothingham *et al.*, 2002).

State-of-the-art numerical models provide powerful analytical tools for predicting river behavior under a variety of management scenarios.

River dynamics involve complex, incompletely understood interactions among flow, sediment transport and channel form. The capacity to predict these interactions is essential for a variety of river management problems, including channel migration, width adjustment and habitat development. To address this need, Computational Fluid Dynamics (CFD) model increasingly are being used by river engineers, fluvial geomorphologists and river biologists to explore the complexity of river dynamics and predict fluvial behavior. Until recently, the application of CFD models was constrained to fairly simple hydrodynamic problems. However, advances in computational capabilities have led to the use of these models to simulate flow in a variety of reach-scale river environments, including straight reaches (Naot *et al*., 1993; Crowder and Diplas, 2000; Nicholas, 2001), stream confluences (Weerakoon and Tamai, 1989; Lane *et al*., 1999; Bradbrook *et al*., 2002) and river bends (Wu *et al*., 1997; Hodkinson and Ferguson, 1998).

The simulation of field-scale conditions with CFD models raises a host of issues that have yet to be adequately resolved. First, the amount and quality of field data required for domain representation, boundary condition specification and model calibration/validation increases considerably with model sophistication. CFD modeling typically requires high-resolution information on the morphology of hydraulic boundaries, which strongly influence flow behavior. Whereas the boundaries of artificial systems often can be represented with quantitative expressions that allow an accurate representation of boundary morphology, the complexity of natural-river boundaries often precludes either a mathematical representation of the boundary or the collection of sufficient field data to capture all details of the boundary.

The complexity of natural rivers also complicates requirements for flow data. Advanced CFD models can predict flow in three dimensions, but until recently field data on 3-D velocity fields were not available. Thus, although a few applications have predicted flow patterns in natural rivers, these predictions have not been verified using field data. Advances in measurement technology now allow 3-D velocity data to be collected in the field (e.g. Rhoads and Sukhodolov, 2001), thereby providing information for model calibration and verification.

The concern about data quality also includes the issue of representativeness. To be useful for modeling purposes, an appropriate data set must represent a well-defined flow condition. For example, CFD models are often utilized to stimulate steady flows and ideally steady-flow data should be used for model validation. Conforming to this requirement is not as simple as it may seem for those accustomed to working in the laboratory. Current field technology does not allow 'snapshot'-type measurements of 3-D velocities for an entire river reach. Collection of a comprehensive set of data can take days, a period during which discharge will change to some extent and, in some cases, may change considerably. Unlike measurements in a controlled laboratory environment, field measurements must be

carefully orchestrated to minimize flow unsteadiness, while recognizing that complete control of flow conditions is impossible. Instead, a balance must be sought between the amount of data deemed suitable for addressing project objectives and the uniformity of the conditions under which the data are acquired.

Second, a numerical model should be able to represent the main processes controlling the flow for a specific situation. In many cases, the treatment of turbulence, boundary roughness and the water surface can have important effects on model predictions. k-ε isotropic turbulence closures perform reasonably well in many natural flows, but a more elaborate closure scheme in necessary in regions of high shear where turbulence anisotropy is important, like shear layers at confluences (Bradbrook *et al*., 1998; Sukhodolov and Rhoads, 2001) and separation zones in meanders (Hodkinson and Ferguson, 1998). Roughness in most models is accounted for using wall functions, which result in maximum turbulent kinetic energy (TKE) levels at the bed. While this assumption is acceptable for sand bedded streams, rivers with gravel or cobbles have high relative roughness, which has been shown to produce a displacement of the peak TKE away from the bed (López, 1997). Empirical modifications of wall functions (López, 1997), high-resolution bed-elevation data (Nicholas, 2001) or artificial-porosity (Olsen and Stokseth, 1995) may be needed to capture this effect. The rigid-lid assumption has been used extensively to account for the water surface in river simulations. This approach replaces the general non-planar free surface with a virtual parallel to the channel bed (Leschziner and Rodi, 1979). Displacements of the free surface can be obtained from pressure computations at the lid, but the results are only acceptable for superelevations of less than 10% of the total channel depth. A more accurate treatment of the water surface is required when the flow is near critical conditions and either surface waves or hydraulic jumps develop.

Third, because of the large amount of information manipulated, either during the preparation of the simulation or at the time of analyzing the model results, data pre- and post-processing procedures are as important as modeling considerations in assessing model performance. Efficient and reliable procedures must be developed to ensure congruence between physical and computational domains. For example, topographical data collected in the field typically are irregularly spaced, whereas computational grids are usually structured. As a result, data pre-processing is required to interpolate information at computational nodes from the surveyed data. If an interpolation method is applied without consideration of its underlying assumptions, it can generate artificial features in regions where information is scarce. Accurate interpolation is also necessary when extracting results at specific locations from the massive volumetric output generated by the model.

All of the major challenges for CFD modeling of natural-river processes are manifested in the application of these models to meandering rivers. Although meandering is a characteristic property of many streams throughout the world, the underlying processes governing this phenomenon have yet to be adequately elucidated and changes in meanders at the reach scale have yet to be accurately predicted.

The complexity of meandering centers on the highly three-dimensional nature of fluid movement and the interaction between the 3-D motion and channel curvature via the mechanics of sediment transport and bank erosion. Three dimensionality of the flow results from the local imbalance over depth between curvature-induced centrifugal forces and the counteracting pressure-gradient force generated by superelevation of the water surface along the outer bank of the bend (Yen and Yen, 1971; Dietrich, 1987). This local force imbalance leads to helicity of the flow that is expressed as a circulation in a plane perpendicular to the local channel direction. Over depth, 3-D time-averaged vectors shift systematically in alignment, with near-surface vectors oriented toward the outer bank and near-bed vectors oriented toward the inner bank. Patterns of 3-D fluid motion within meandering rivers have been related to meander development and evolution (Rhoads and Welford, 1991). Of particular importance is the effect of curvature on enhancing velocity magnitudes close to the outer bank. In bends, near-bank velocities govern both erosion of the outer bank and aggradation of the inner bank, and are used to compute migration rates in models of planform evolution (Ikeda *et al*., 1981; Johanesson and Parker, 1989; García *et al*., 1994). Flow in a natural meandering channel also interacts with other topographic features, generating a wide variety of 3-D patterns of fluid motion as water moves through pools, riffles and emergent vegetation or around point bars, slump blocks and large woody debris. This geomorphic diversity provides a variety of habitat elements for aquatic organisms and has been related to fish abundance and biomass (Frothingham *et al*., 2001), providing an established linkage among stream geomorphology, hydraulics and ecology.

This paper presents numerical simulations of flow through a natural meandering river using two different models: a depth-averaged numerical code with secondary flow correction and a fully 3-D, state-of-the-art Computational-Fluid-Dynamics (CFD) code. The scale of the problem examined here is in the overlapping domain of applicability of the two models, providing a basis for moving from these simulations both to larger- and smaller-scale analyses. The 2-D model generates only depth-averaged results and can be applied to large spatial domains, while the 3-D model generates a complete and detailed picture of the flow field, but at the expence of considerable computational time. In fact, the numerical simulation is rather ambitious for application of a full 3-D CFD model, as demonstrated by the lack of previous simulations at the scale and degree of complexity of the reach examined in this study. Neither of the models has been applied at the field-scale using data for a natural meandering stream. Computational grids for both models are developed using field data on channel topography for a highly sinuous reach of the Embarras River, a small meandering stream in East Central Illinois. Hydraulic boundary conditions are based on measured flows in the reach and model predictions are compared to 3-D velocity data collected in the reach.

2. Numerical Models

2.1. STREMR

STREMR is a hydrodynamic model developed at the Waterways Experimental Station of the U.S. Army Corps of Engineers (Bernard, 1993). It solves the depth-averaged incompressible Navier-Stokes equations in a curvilinear grid using finite volumes. Conservation of momentum and mass are given, expressed herein in Cartesian coordinates for the sake of simplicity, respectively by (Bernard, 1993):

$$\frac{\partial \overline{u}_i}{\partial t} + \overline{u}_j \frac{\partial \overline{u}_i}{\partial x_j} = -\frac{1}{\rho}\frac{\partial p}{\partial x_i} + T_i - X_i + S_i \tag{1}$$

$$\frac{\partial (h\overline{u}_i)}{\partial x_i} = 0 \,, \tag{2}$$

where $\overline{u}_i$ is the depth-averaged velocity component in the i-th direction (i goes from 1 to 2, with components $\overline{u}$ and $\overline{v}$), t is the time, x_i is the spatial coordinate in the i-th direction (namely x and y), ρ is the density, p is the pressure, and h is the water depth. In turn, T_i, X_i, and S_i refer to the viscous, friction and secondary-flow forces in the i-th direction. Viscous forces have been parameterized as follows:

$$T_x \approx h^{-1}\tilde{\nu}_t \nabla\cdot(h\nabla\overline{u}) + 2\frac{\partial \tilde{\nu}_t}{\partial x}\frac{\partial \overline{u}}{\partial x} + \frac{\partial \tilde{\nu}_t}{\partial y}\left(\frac{\partial \overline{u}}{\partial y} + \frac{\partial \overline{v}}{\partial x}\right) \,, \tag{3}$$

and

$$T_y \approx h^{-1}\tilde{\nu}_t \nabla\cdot(h\nabla\overline{v}) + 2\frac{\partial \tilde{\nu}_t}{\partial y}\frac{\partial \overline{v}}{\partial y} + \frac{\partial \tilde{\nu}_t}{\partial x}\left(\frac{\partial \overline{v}}{\partial x} + \frac{\partial \overline{u}}{\partial y}\right) \,, \tag{4}$$

with $\overline{\nu}_t$ referring to the depth-averaged kinematic eddy viscosity.

The friction force is represented through Manning's n,

$$X_i = \frac{C_f}{h}\overline{u}_i|\underline{\overline{u}}| = \frac{gn^2}{h^{4/3}}\overline{u}_i|\underline{\overline{u}}| \,, \tag{5}$$

where $|\underline{\overline{u}}|$ is the modulus of the depth-averaged velocity vector, and C_f is the friction coefficient.

Finally, the secondary-flow force is given by:

$$S_i \approx \frac{1}{\rho}\frac{\overline{u}_i}{|\underline{\overline{u}}|}\left[h^{-1}\underline{n}\cdot\nabla(h\tau_s) + 2\frac{\tau_s}{r}\right] \,, \tag{6}$$

where τ_s is the depth-averaged shear stress produced by the secondary circulation, $\underline{n}$ is the unit vector normal to the velocity vector, and r is the streamline curvature radius. Turbulence stresses are simulated using a k-ε model (Rodi, 1984) and secondary stresses are accounted for by solving an additional equation for Ω,

a surrogate for the depth-averaged streamwise vorticity. The transport equations for the depth-averaged turbulence kinetic energy, $\tilde{k}$, dissipation rate, $\tilde{\varepsilon}$, and Ω are (Bernard, 1993):

$$\frac{\partial \tilde{k}}{\partial t} + \overline{u}_j \frac{\partial \tilde{k}}{\partial x_j} = \tilde{\nu}_t \left(\frac{\partial \overline{u}_i}{\partial x_j} + \frac{\partial \overline{u}_j}{\partial x_i} \right) \frac{\partial \overline{u}_i}{\partial x_j} + \\ + \frac{1}{\sigma_k} \left[h^{-1} \tilde{\nu}_t \nabla \cdot \left(h \nabla \tilde{k} \right) + \nabla \tilde{\nu}_t \cdot \nabla \tilde{k} \right] - \tilde{\varepsilon} \tag{7}$$

$$\frac{\partial \tilde{\varepsilon}}{\partial t} + \overline{u}_j \frac{\partial \tilde{\varepsilon}}{\partial x_j} = c_1 \frac{\tilde{\varepsilon}}{\tilde{k}} \tilde{\nu}_t \left(\frac{\partial \overline{u}_i}{\partial x_j} + \frac{\partial \overline{u}_j}{\partial x_i} \right) \frac{\partial \overline{u}_i}{\partial x_j} + \\ + \frac{1}{\sigma_\varepsilon} \left[h^{-1} \tilde{\nu}_t \nabla \cdot (h \nabla \tilde{\varepsilon}) + \nabla \tilde{\nu}_t \cdot \nabla \tilde{\varepsilon} \right] - c_2 \frac{\tilde{\varepsilon}^2}{\tilde{k}} \tag{8}$$

$$\frac{\partial \Omega}{\partial t} + \overline{u}_j \frac{\partial \Omega}{\partial x_j} = A_s \sqrt{C_f} \frac{|\overline{u}|^2}{rh} - D_s \sqrt{C_f} \Omega \frac{|\overline{u}|}{h} + \\ + h^{-1} \tilde{\nu}_t \nabla \cdot (h \nabla \Omega) + \nabla \tilde{\nu}_t \cdot \nabla \Omega \, , \tag{9}$$

where c_1, c_2, σ_k, σ_ε, A_s and D_s are empirical coefficients. The turbulent kinetic energy and the turbulence dissipation rate are combined to compute the eddy viscosity as:

$$\tilde{\nu}_t = c_\nu \frac{\tilde{k}^2}{\tilde{\varepsilon}} \, , \tag{10}$$

where c_ν is also empirically obtained. In turn, Ω is related to the depth-averaged streamwise vorticity, $\overline{\omega}_s$, by:

$$\Omega = c_{2\omega} \frac{\overline{\omega}_s}{12} \, , \tag{11}$$

with $c_{2\omega}$ being a constant of proportionaliy. Note that $\tilde{\nu}_t$, $\tilde{k}$ and $\tilde{\varepsilon}$ correspond to a depth-averaged formulation and are different from the local values of ν_t, k and ε used in a 3-D analysis.

The water surface is approximated as a rigid lid, and the pressure in this surface is then converted to water-surface elevation values. The equations are solved in a curvilinear boundary-fitted grid, which requires the use of a grid generator. Results of the model show a reasonable agreement with measurements on laboratory bends (Bernard, 1993), and on a braided river (Lane *et al.*, 1995).

2.2. FLOW-3D®

FLOW-3D®, developed by Flow Science, Inc., solves the fully 3-D transient Navier-Stokes equations by a finite-volume-finite-differences method in a fixed Eulerian

rectangular grid. The model adopted in this case is based on the numerical integration of the conservation equations for momentum and mass, in the following form (again, in Cartesian coordinates):

$$\frac{\partial u_i}{\partial t} + \frac{\partial u_i}{\partial x_j} = \frac{1}{\rho}\frac{\partial p}{\partial x_i} + G_i - \frac{\tau_{bi}}{\rho} + \frac{1}{\rho}\frac{\partial \tau_{ij}}{\partial x_j} \tag{12}$$

$$\frac{\partial u_i}{\partial x_i} = 0\,, \tag{13}$$

where u_i is the velocity component in the i-th direction (i goes from 1 to 3), t is time, x_i is the spatial coordinate in the i-th direction, p is the pressure, ρ is the local density, G_i are the body accelerations (coming from body forces), τ_{ij} are the viscous stresses and τ_{bi} is the wall shear stress (only activated close to solid boundaries).

Although not specifically devised for river problems, the model includes features that are important for the simulation of open channel flows in natural and artificial basins, which allow for an accurate treatment of turbulence, water surface and solid boundaries. If the Reynolds-averaged Navier-Stokes (RANS) equations are solved, a variety of turbulent closures can be chosen, including mixing length theory, one equation model, two equation (k-ε) model and Renormalization Group Theory (RNG). This last closure represents an improvement over the standard k-ε model – widely used in computational hydraulics during the seventies – and performs better in situations of high shear and separation zones. The RNG turbulent closure is represented by the following transport equations for k and ε:

$$\frac{\partial k}{\partial t} + u_j\frac{\partial k}{\partial x_j} = \nu_t\left(\frac{\partial u_i}{\partial x_j} + \frac{\partial u_j}{\partial x_i}\right)\frac{\partial u_i}{\partial x_j} + \frac{\partial}{\partial x_j}\left(\alpha_k \nu_{eff}\frac{\partial k}{\partial x_j}\right) - \varepsilon \tag{14}$$

$$\begin{aligned}&\tfrac{\partial \varepsilon}{\partial t} + u_j\tfrac{\partial \varepsilon}{\partial x_j} = \\ &c_{\varepsilon 1}\tfrac{\varepsilon}{k}\nu_t\left(\tfrac{\partial u_i}{\partial x_j} + \tfrac{\partial u_j}{\partial x_i}\right)\tfrac{\partial u_i}{\partial x_j} + \tfrac{\partial}{\partial x_j}\left(\alpha_\varepsilon \nu_{eff}\tfrac{\partial \varepsilon}{\partial x_j}\right) - c_{\varepsilon 2}\tfrac{\varepsilon^2}{k} - R\end{aligned} \tag{15}$$

with

$$R = \frac{c_\mu \eta^3\left(1 - \dfrac{\eta}{\eta_0}\right)\varepsilon^2}{(1 + c_3\eta^3)k} \tag{16}$$

$$\nu_{eff} = \nu_t\left[1 + \sqrt{\frac{c_\mu k}{\mu\sqrt{\varepsilon}}}\right]^2 \tag{17}$$

$$\eta = \sqrt{\left(\frac{\partial u_i}{\partial x_j} + \frac{\partial u_j}{\partial x_i}\right)\frac{\partial u_i}{\partial x_j}}\frac{k}{\varepsilon} \tag{18}$$

where ν_t is the eddy viscosity, μ is the dynamic viscosity of the fluid and $c_{\varepsilon 1}$, $c_{\varepsilon 2}$, c_3, α_k, α_ε, η_0 and c_μ, are constants. The RNG theory predicts $c_{\varepsilon 1} = 1.42$, $c_{\varepsilon 2} = 1.68$, $c_3 = 0.012$, $\eta_0 = 4.38$ and $c_\mu = 0.085$, whereas α_k and α_ε are of order 1. In this model, turbulence is more sensitive to the mean rate of strain than the standard k-ε model, due to the presence of the term R.

Free surface boundaries and fluid interfaces are treated using the Volume-of-Fluid (VOF) technique (Hirt and Nichols, 1981). The free surface is not only unknown in 3-D computations, but it also acts a boundary for the problem. The matter is not only one of locating the free surface in a 3-D Eulerian grid, but also of keeping a sharp representation of the interface and, overall, doing it effectively in terms of computational time. VOF is based on the definition of a function F (volume fraction), whose value at any grid-point is 1 if occupied by fluid and 0 if not. F is, then, a continuous function bounded by 0 and 1, and it is governed by the following convection transport equation:

$$\frac{\partial F}{\partial t} + \frac{\partial (F u_j)}{\partial x_j} = 0 \,. \tag{19}$$

A null tangential stress boundary condition is imposed at the free surface. The VOF technique is both accurate and effective, since it only requires computation and storage of one additional variable (F). A discussion about the issues related to the VOF method can be found in Bombardelli *et al*. (2001).

Another distinctive feature of the model, the Fractional – Area – Volume – Obstacle – Representation (FAVOR) technique (Hirt and Sicilian, 1985), allows for the definition of solid boundaries within the Eulerian grid. FAVOR determines fractions of areas and volumes (open to flow) in partially blocked volumes, for the computation of fluxes in concomitance with those boundaries. In this way, the process of defining boundaries and obstacles is done independently of grid generation, avoiding saw-tooth representation or the use of body fitted grids. In fact, the geometry can be defined using a built-in 'solid modeler', which includes quadratic functions that represent objects, or it can be externally provided through CAD or ANSYS formats. Once the geometry has been defined, the computational mesh is constructed indepently, with the possibility of densification in zones of the domain of particular interest.

3. Application

3.1. THE FIELD SITE

The Embarras River originates at the southern edge of Champaign-Urbana, Illinois and flows south through a low-relief agricultural landscape. The study site consists of a 70 m long meander loop within a highly sinuous section of the river (Figure 1). Over the past 60 yr, this loop has evolved from a simple bend into a double-headed loop, or composite bend. The current configuration consists of

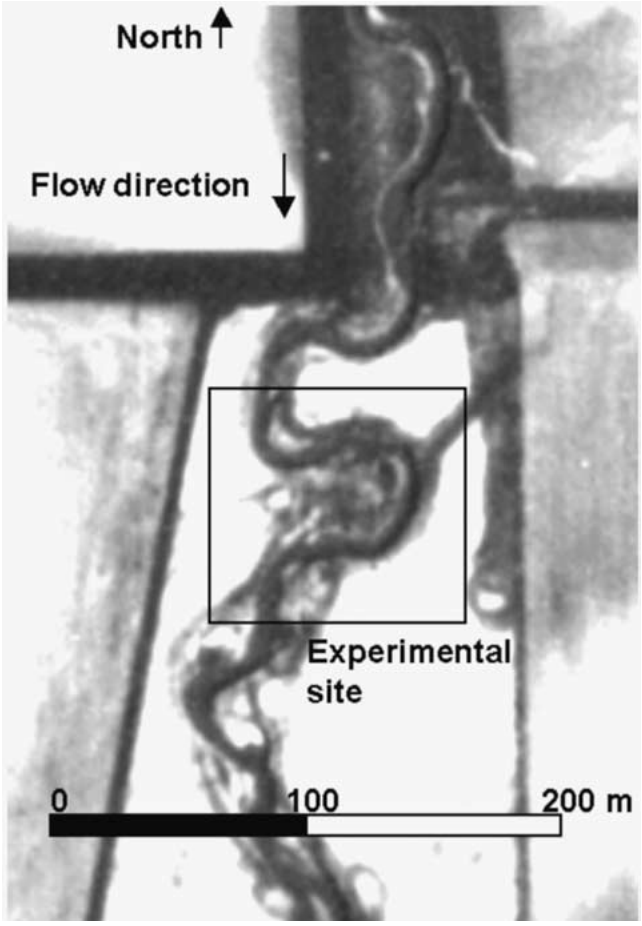

Figure 1. Aerial photo of the Embarras River showing the experimental site.

two separate consecutive bends curving in the same direction connected by a short straight reach (Figure 2). The field data used to evaluate the predictive capabilities of the numerical models consist of topographic survey information and 3-D velocity measurements obtained within the study reach on 5 and 8 June 1998 (Frothingham, 2001). Low-flow conditions (approx. 1 m^3 s^{-1}) prevailed during the measurements. The reach was surveyed at 14 cross sections (numbered 1 to 14 in Figure 2) spaced approximately every 5 m, and oriented orthogonally to the bankfull channel direction. Elevations were referred to a local datum and ranged from 8 to 10 m. Transverse spacing of the topographic survey locations was typically 0.5 to 1.0 m, except where abrupt changes in slope dictated a finer spacing. Three-dimensional velocity measurements were collected with an Acoustic Doppler Velocimeter (ADV) at 10 of the 14 cross sections (4–9, 11–14). Velocities were measured at several verticals (seven to eight) and at several points in the vertical (two to eight) over a time interval long enough to ensure 60–90 sec of

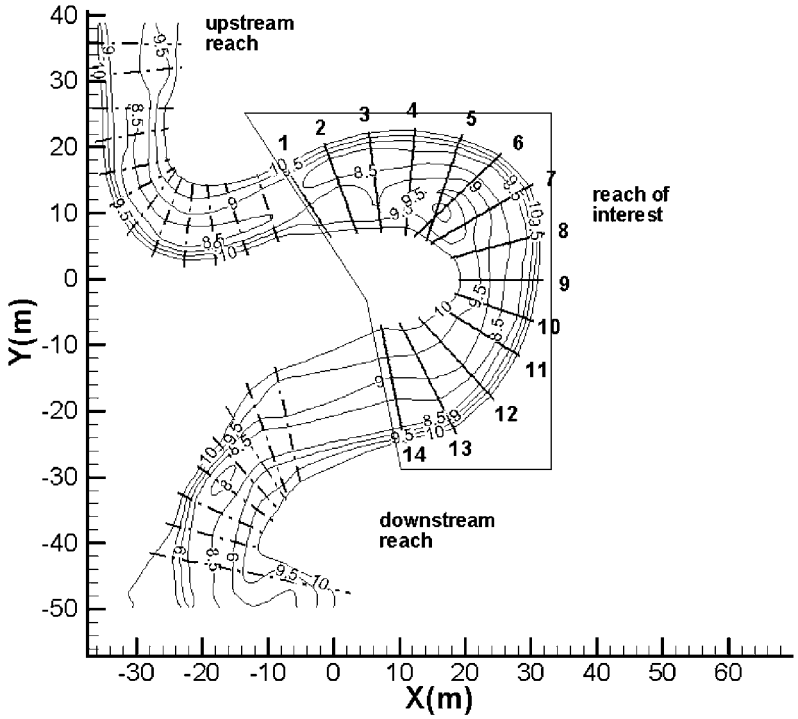

Figure 2. Plan view of the experimental reach showing contour lines and location of the cross sections.

representative measurements at each point, using a 25 Hz sampling frequency. The bed sediment is a mix of sand and small gravel throughout the reach with a mean grain size of 0.84 mm.

3.2. THE COMPUTATIONAL DOMAIN

One of the most difficult tasks, when applying a model to a flow in a natural environment, is the definition of the boundary conditions. Even if detailed information for all the required variables were available, the numerical codes will not always have the flexibility to accommodate measured irregular distributions as inputs. To moderate the effects of boundary conditions on the results, it is common practice in computational hydraulics to place buffer zones upstream and downstream of the reach of interest. In this way, any computational inaccuracies induced by uncertainties in boundary-condition specification can be resolved outside of the reach of interest as the solution evolves and the flow interacts with the boundary geometry in the added portions of the computational domain. Since the extension of the computational domain requires extra topographic information as well as more work in terms of meshing and model setup, it is desirable to keep the buffer zones as small as possible. The minimum adjustment distance is hard to define and depends on the

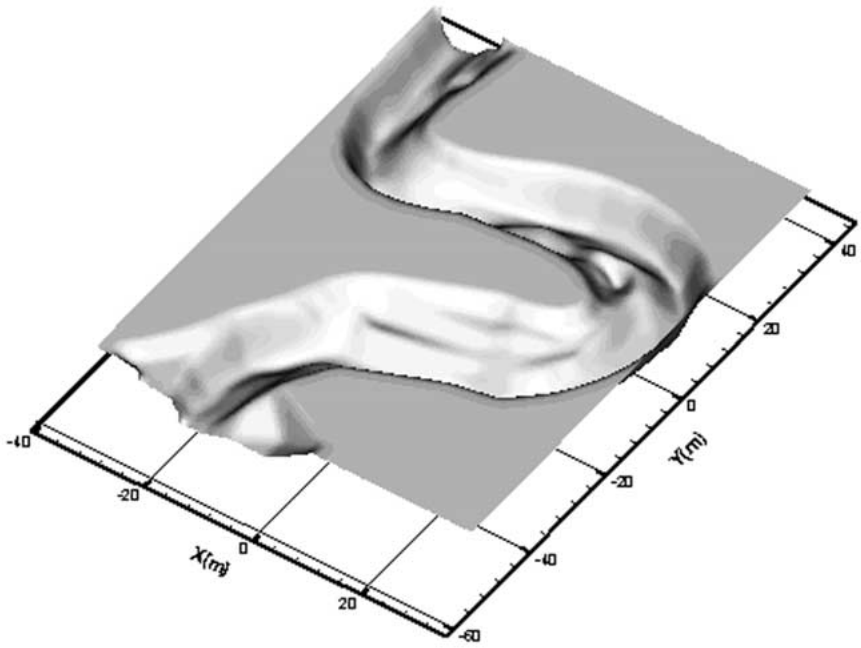

Figure 3. 3-D reconstruction of the terrain surface.

flow characteristics: while in a straight reach a length of 20–40 times the depth may be appropriate, a meandering reach can require substantially longer extensions, particularly at the upstream end. This need for extra length is mainly related to the spiral motion that develops in bends, which results in residual circulation patterns that can influence the flow downstream of a bend at the entrance to the next bend in the meander sequence. Unless a long straight reach exists upstream of a particular bend of interest, which is not the case for the study reach, the effects of upstream bends should be included in the computational domain.

For the present simulations, topographic information from 60 m long sections of the Embarras River upstream and downstream of the study reach (Frothingham, 2001) was added to the computational domain to account for boundary effects (Figure 2). This adjustment length exceeds a distance of 40 times the flow depth (10 m for a 0.5 m average depth) and encompasses two adjacent bends – one upstream and one downstream – of the study reach. Additional tests were performed to verify whether the upstream extension was long enough to capture residual circulation effects. A sequence of two identical meanders was used for this purpose. Due to the similitude between the consecutive meanders in the field (Figure 1), duplicating the domain was less demanding than reconstructing the real upstream topography, yet it provided an acceptable representation of curvature-induced effects for the downstream reach. A similar approach to artificially simulate upstream effects has been used in the past by Nelson and Smith (1989).

3.3. DEPTH-AVERAGED SIMULATION

STREMR input requires the specification of cell depths as well as boundary conditions. The two-meander sequence was first used for the simulations in order to consider the possible influence of the upstream reach. Final runs were carried out on the downstream meander only, using a dense curvilinear boundary-fitted grid with a grid cells size of 0.1×0.1 m in the streamwise and spanwise directions, respectively. Although the program has some capabilities of handling non-regularly spaced topographic data, depths at all the grid points were generated externally using graphic software to guarantee a precise interpolation (Figure 3). A triangulation was first performed relating the surveyed points, to then apply linear interpolation and obtain grid-point values. The topography generated by this procedure was compared with hand-contoured maps, showing a correct representation of the main morphological characteristics of the reach. In fact, the basic principles of both methodologies are essentially the same, so the agreement was not surprising.

Upstream boundary conditions were defined in terms of flow discharge and position of the rigid lid, which coincided with the observed water level. Additionally, for the transport Equations (7) to (9), the normal derivatives of k and ε, as well as the value of Ω were assumed to be zero in input boundaries. Manning's n was varied in order to match the observed water levels and depth-averaged velocities. The coefficients involved in the turbulence and secondary flow computations (Equations (7) to (9)) were set at the model's standard values, i.e., $c_1 = 1.44$, $c_2 = 1.92$, $\sigma_k = 1.0$, $\sigma_\varepsilon = 1.3$, $A_s = 5.0$, $D_s = 0.5$ and $c_\nu = 0.09$ (Bernard, 1993).

3.4. 3-D SIMULATION

FLOW-3D® defines the geometry of the problem either using its own solid modeler or interpreting solid objects generated by other programs. Use of the solid modeler was impractical to represent the irregular natural topography because it requires objects to be defined as a combination of general quadratic functions. Instead, the data of the cross sections were interpolated to a regular grid using graphic software (as for the 2-D modeling) and then converted into a 3-D solid object (Stereolithography) using AUTOCAD. The grid size of the topography was 0.25×0.25 m in the x and y directions, respectively.

Two sets of numerical experiments were carried out. The first set used the two-meander sequence whereas the second included only the downstream meander, but using a much denser grid with representative cell sizes of $0.25 \times 0.62 \times 0.023$ m in the x, y and vertical directions, respectively. Water levels at the upstream and downstream boundaries were initially set to values of stage obtained from the measurements on the reach. The RNG turbulence closure was adopted and the roughness parameter k_s was adjusted until depths and velocities matched the observations.

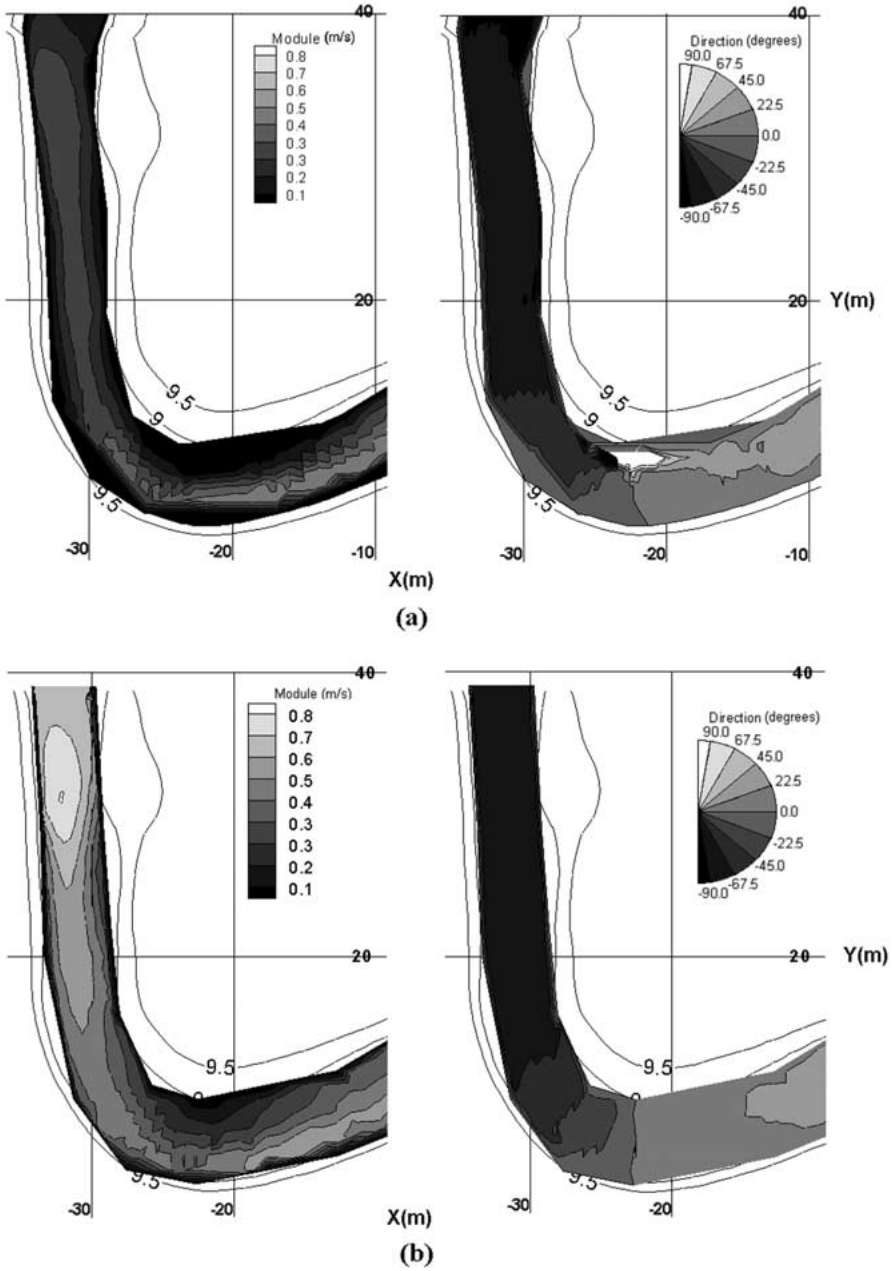

Figure 4. Depth-averaged velocities at the entrance of the study region using STREMR: (a) with upstream meander, (b) without upstream meander.

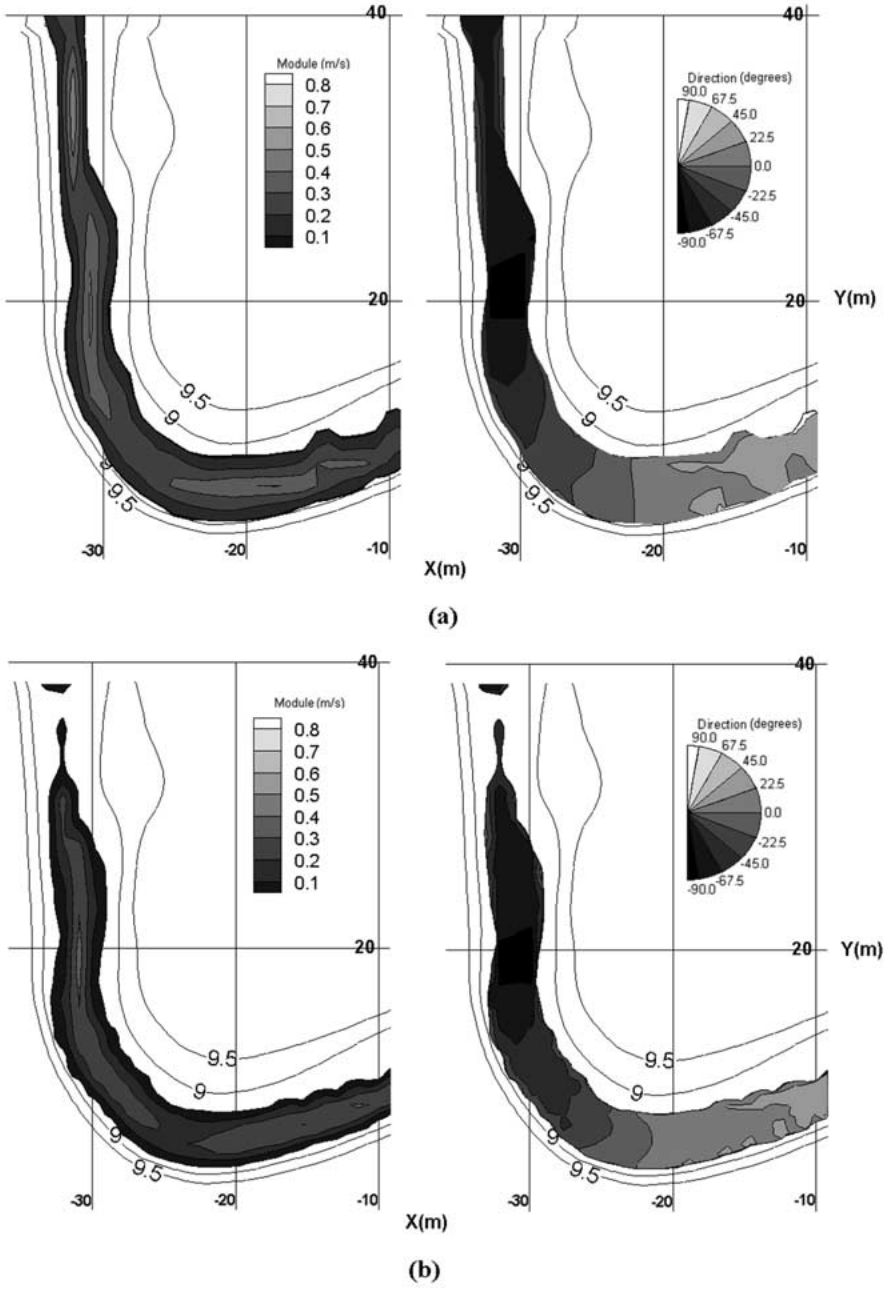

Figure 5. Near-bed velocities at the entrance of the study region obtained using FLOW-3D®: (a) with upstream meander, (b) without upstream meander.

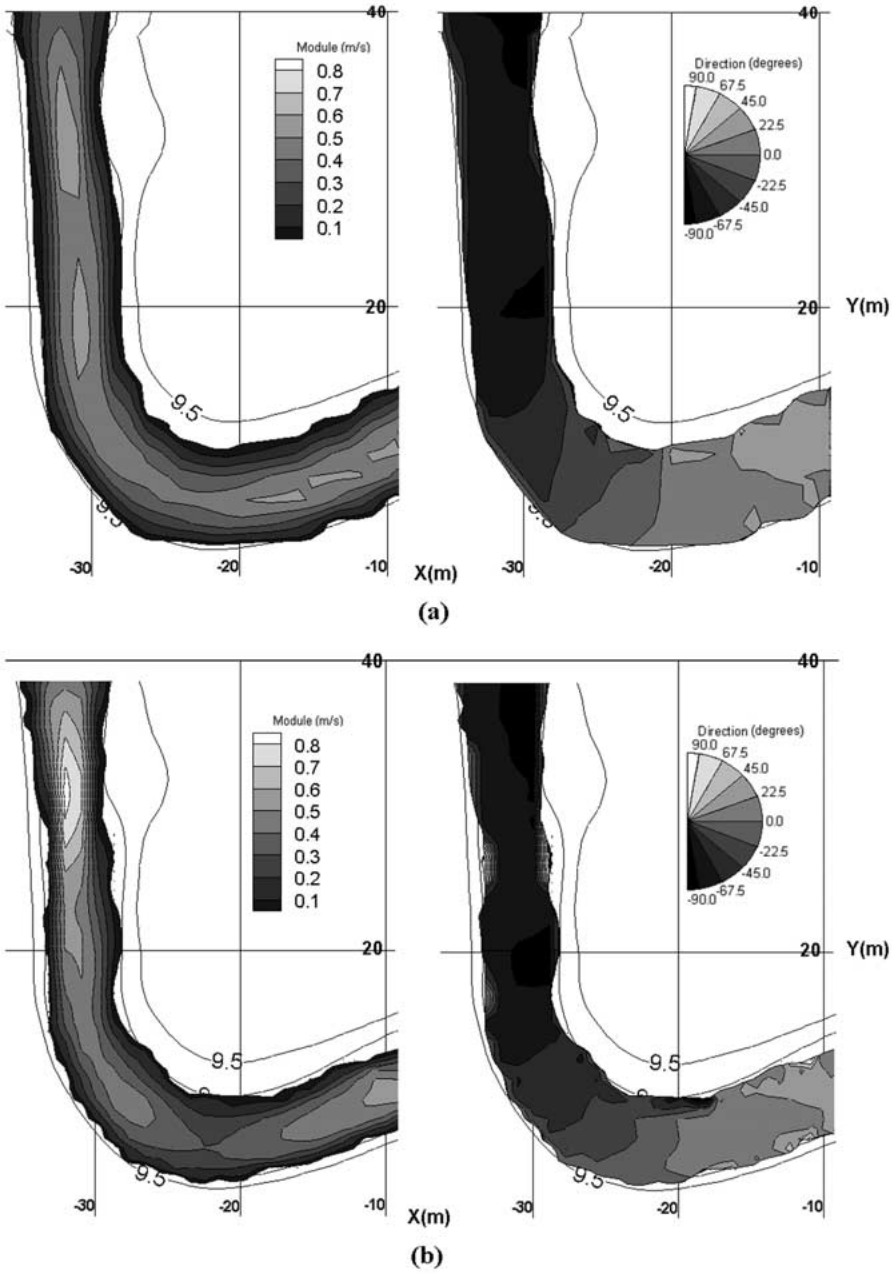

Figure 6. Near-surface velocities at the entrance of the study region obtained using FLOW-3D®: (a) with upstream meander, (b) without upstream meander.

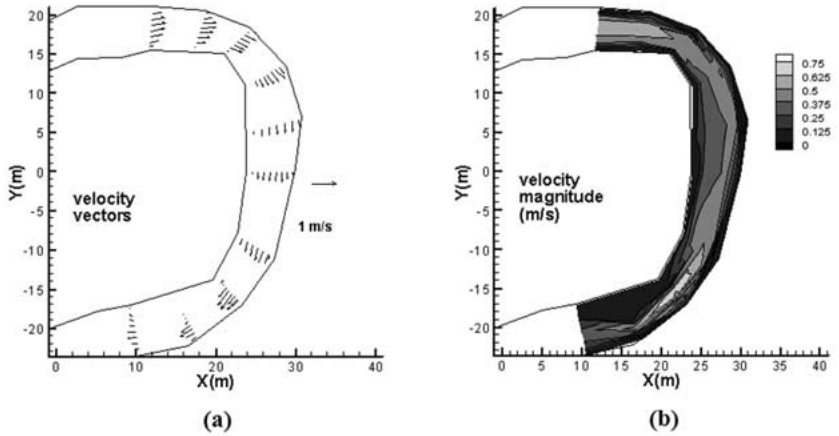

Figure 7. Depth-averaged velocity field obtained from measurements: (a) vectors, (b) contours of magnitude.

4. Analysis of the Results

4.1. INFLUENCE OF THE UPSTREAM REACH

Initial runs carried out on the two-meander sequence, both with the depth-averaged and the 3-D model, showed that the presence of the upstream meander did not substantially affect the numerical results on the study reach. Figures 4 to 6 compare the entrance region of the study area, with and without the inclusion of the upstream meander, in terms of depth-averaged (Figure 4), near-bottom (Figure 5) and near-surface velocities (Figure 6). Figure 4 corresponds to STREMR results whereas Figures 5 and 6 were obtained using FLOW-3D®. In all cases, differences in the incoming velocity ditributions are significantly attenuated as the flow goes through the bend, resulting in very similar patterns at the exit. At the exit cross-section, differences in velocity magnitude are 20, 24 and 18% for Figures 4, 5 and 6, respectively. Based on these results, subsequent simulations were performed on the downstream meander only.

4.2. DEPTH-AVERAGED RESULTS

Model results correspond to a uniform n value of 0.035, which is consistent with values proposed elsewhere (Chow, 1959) for streams with hydraulic characteristics similar to those of the study reach. Depth-averaged velocities obtained from the field measurements are presented in the form of a vector plot (Figure 7a) and a contour plot of the velocity distribution (Figure 7b). Despite the rather large spacing between consecutive measurement sections, a contour plot was chosen as the best way to present the data for purposes of comparison. Figures 8a and b present results obtained from STREMR. The model predictions are reasonable in terms of

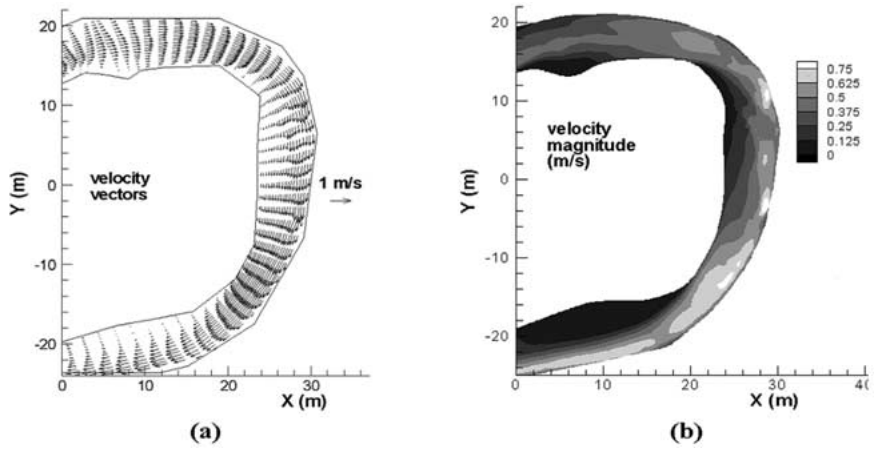

Figure 8. Depth-averaged velocity field obtained with STREMR: (a) vectors, (b) contours of magnitude.

magnitude as well as general direction of the depth-averaged velocities. Relative errors computed at the cross sections with velocity measurements are below 30% on average, with the higher values at cross sections 7 and 10 and close to the banks. Both the field data and model results show that the highest velocities are located towards the outer bank within the bends, whereas low velocities occur along the inner banks within the bends. The model accurately reproduces a region of recirculation along the inner bank downstream of the second bend.

4.3. 3-D RESULTS

A uniform roughness value of $k_s = 5$ mm was found to give the best results in the 3-D simulations. For uniform material over a flat bed k_s should fall between 1 and 3 times the sediment diameter, which would give a value between 1 and 3 mm if the mean diameter of the reach were used. However, roughness produced by non-uniform material tends to be dominated by the coarser grains resulting in a larger effective k_s.

Depth-averaged velocities computed from the FLOW-3D® results are presented in the form of vector and contour plots of the velocity magnitude (Figures 9a and b). In Figure 9a, only some of the vectors have been drawn for the sake of clarity. Velocities measured in the field at some of the cross sections are presented as vector plots of the transverse velocity field (Figure 10a) and contour plots of the streamwise velocity distributions (Figure 10b). Estimated transverse and streamwise velocities for the 3-D simulations are presented in Figures 11a and b. In these plots, cross sections must be interpreted looking upstream, i.e., the inner bank is on the left part of the figures.

The model velocities of Figure 9 show a pattern similar to that of the measurements (Figure 7). Relative errors are higher at cross sections 7 and 9 and close to the

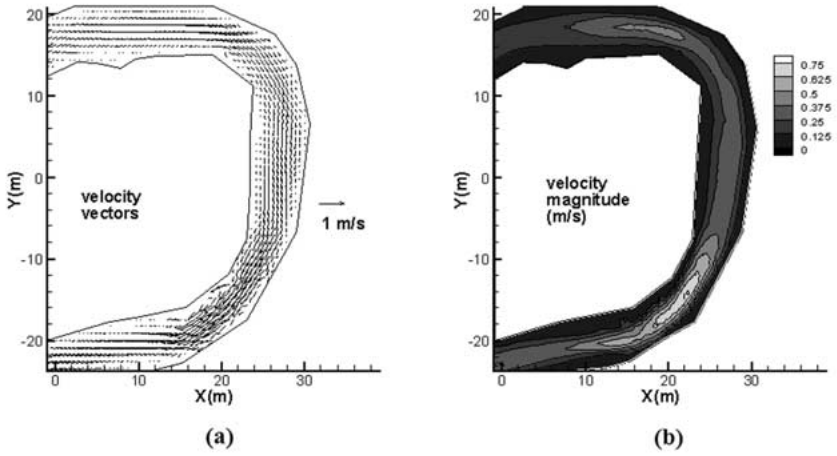

Figure 9. Depth-averaged velocity field obtained with FLOW-3D®: (a) vectors, (b) contours of magnitude.

banks, with an average of 35%. The model accurately predict the main characteristics of the flow field (Figures 10 and 11). Just before entering the first bend (section 5) there is a substantial transverse velocity component towards the outer bank due to centrifugal effects. As the flow enters the bend, helical flow develops (section 7) leading to submergence of the high-velocity core beneath the water surface. In the straight connecting reach (section 9) the flow is almost unidirectional with a small residual transverse current towards the inner bank. A similar sequence is observed in the second bend (sections 12 and 14). At section 14 the combined effect of flow convergence along the outer bank and abrupt channel widening produces a zone of recirculation on the inner bank. All these elements of the flow field are present in the simulations of Figure 11, although the helical flow and the associated submergence of the zone of maximum velocities at section 7 are not as pronounced as in the field data. Underprediction of secondary circulation patterns is rather common in numerical models with isotropic turbulent closures like RNG, which are not very efficient in capturing secondary circulation due to turbulence anisotropy at the walls (bed and banks). The model predicts the recirculation zone near section 14, but the size of the zone is slightly smaller than the measured one (Figure 11).

5. Conclusions

Results of the numerical simulations show that both STREMR, a depth-averaged 2-D model, and FLOW-3D®, a fully 3-D model, accurately predict the main characteristics of the measured velocity field. The agreement is remarkable for a field situation, where sources of uncertainty are multiple and derive from the data and the modeling itself.

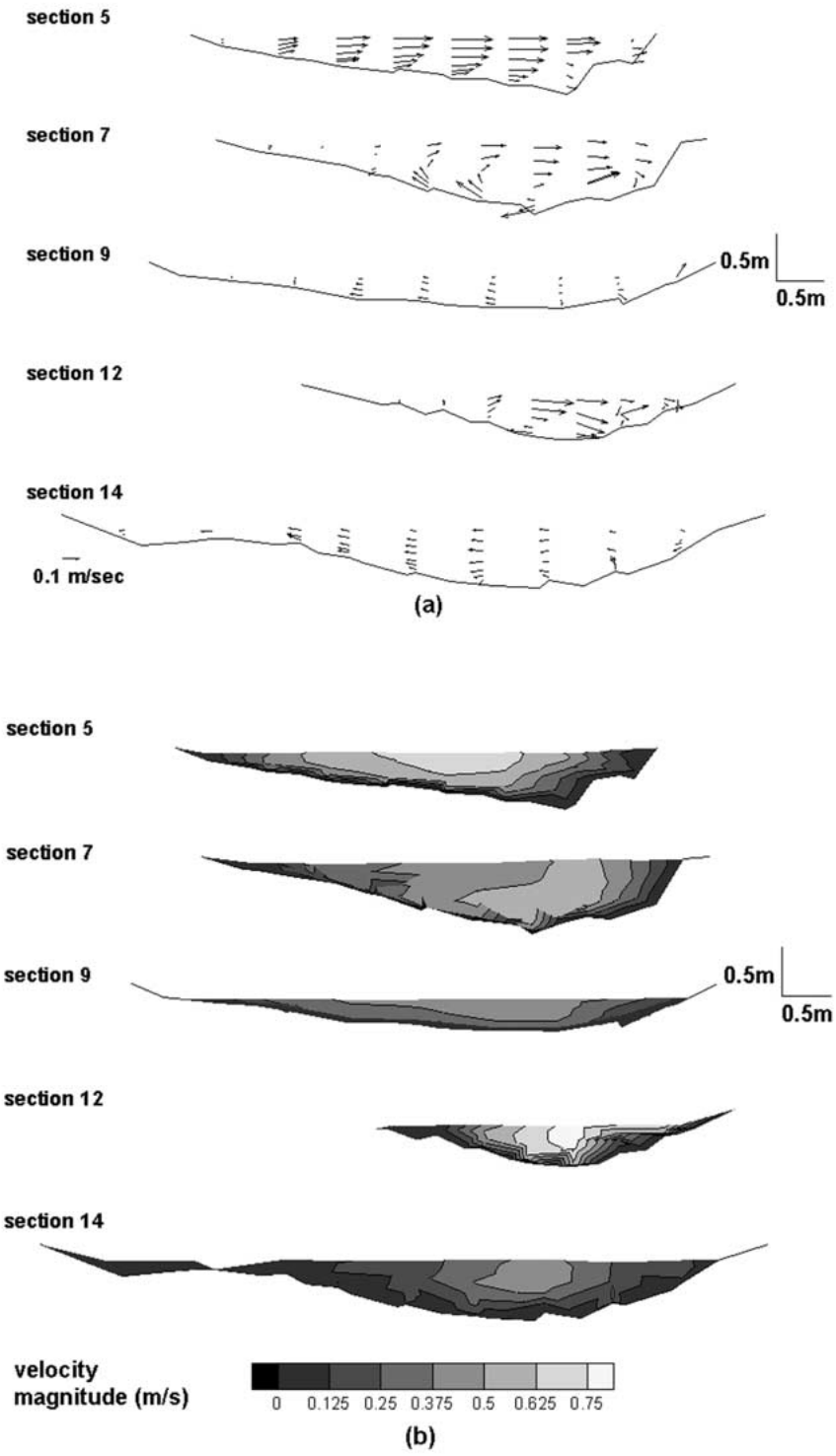

Figure 10. Measured velocities at the cross sections: (a) transverse component, (b) magnitude.

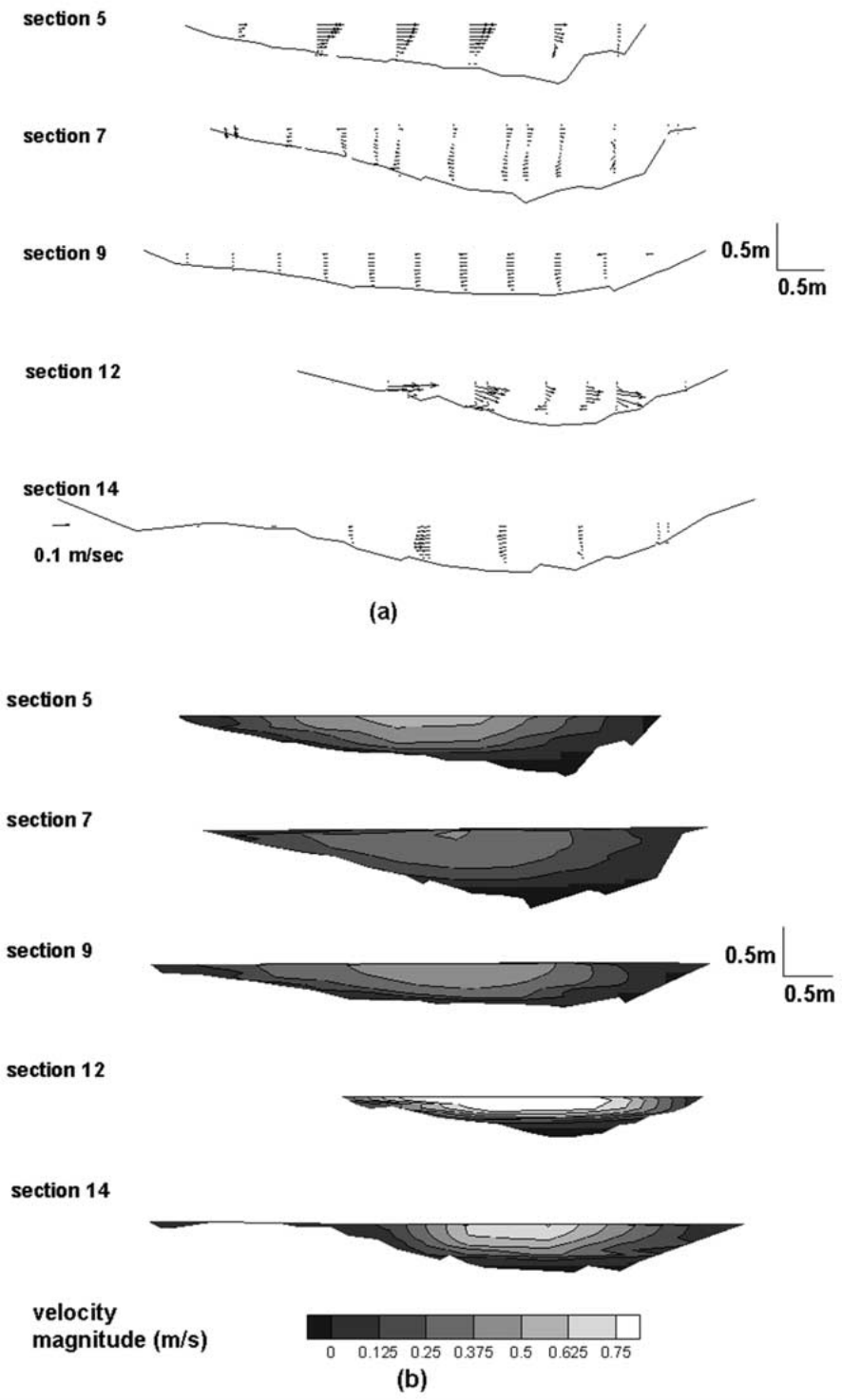

Figure 11. FLOW-3D® results at the cross sections: (a) transverse component, (b) magnitude.

Regarding the depth-averaged modeling, the combination of rigid lid approximation, together with k-ε turbulence closure, roughness characterization and secondary flow correction provides a fast and reliable tool to assess the 2-D dynamics of natural meandering streams. The secondary flow correction is of particular importance, since many depth-averaged models do not account for the transverse redistribution of momentum due to curvature and typically underestimate the magnitude of velocities in the outer part of bends (Finnie *et al*., 1993).

On the other hand, modeling of the 3-D dynamics requires more accurate treatments of both turbulence and water surface. FLOW-3D® results show that the RNG turbulence closure combined with the VOF surface tracking method can accurately predict separation zones as well as 3-D patterns of fluid motion. It must be noted that secondary velocities typically are extremely difficult to predict accurately due to their small magnitudes compared to streamwise velocities.

Perhaps more important than the absolute evaluation of the accuracy of the models in terms of the velocity field is their predictive capability in terms of sediment transport, planform development and habitat structure as inferred from the hydrodynamics. Near-bed velocities are strongly related to patterns of sediment transport and bed morphology. Near-bed flow predicted by FLOW-3D® is directed toward the outer bank upstream of the first bend and then shifts toward the inner bank as helicity develops within the bend. This pattern of flow produces corresponding patterns of sediment movement, with the main pathway of longitudinal sediment transport following the locus of maximum depth-averaged velocities. The combination of a longitudinal increase in near-bed velocity through the bend, which in part reflects submergence of the high-velocity core, the progressive outward shift of the high-velocity core, and the strong lateral flow toward the inner bank produces a sediment flux divergence that accounts for the development of the pool along the outer bank. In turn, the longitudinal decrease in velocity around the inner bank of the bend along with the inward near-bed flow generates a sediment flux convergence that accounts for the development of the point bar. All this features are in agreement with well-known interactions between flow and sediment in river bends.

Planform change is the result of bank erosion, which depends on the near-bank sediment flux associated with spatial patterns of 3-D velocities. The streambanks at the study site have a typical composite structure characterized by cohesive material in the upper bank and exposed sand-gravel in the lower bank. Collapse occurs through gravity-induced failures triggered by toe erosion that occurs when high near-bank velocities mobilize sand and gravel in the lower bank. The zone of maximum near-bank velocities is located near the point of maximum curvature in each bend, as shown both by the field measurements and the model results. This location also marks the maximum pool depth, creating high banks that are prone to collapse. Recent surveys of channel change indicate that the loci of maximum bank erosion in the study reach correspond to the zones of maximum near-bank velocity and pool depth (Frothingham, 2001). Erosion at the outer banks is accompanied

by point-bar accretion on the opposite bank, resulting in a net translation of the meander loop.

From an ecological point of view, flow pattern and channel morphology strongly influence the composition of fish communities in the Embarras River (Frothingham *et al*., 2001). Of particular importance is the high-degree of hydrodynamic variability in the highly sinuous reach, which provides the habitat variability required for different fish species and for various life-history needs of the same species. For example, low velocity areas typicall provide shelter to fish and can be found in deep pools, in separation zones or in the wakes of boulders (Crowder and Diplas, 2000) and large woody debris. For the flow condition analyzed, pools are affected by the submergence of the core of high velocity, limiting its functionality as refuge. However, a separation zone is clearly identifiable following the second bend in both the measurements and the numerical results, with potential for shelter of aquatic biota.

Acknowledgements

This work was supported by Grants from the National Science Foundation (SBR-9811322), the STAR Program of the U.S. Environmental Protection Agency (R82-5306-010) and the Watersheds Program of the U.S. Environmental Protection Agency (R827148-01).

References

Bernard, R. S.: 1993, 'STREMR: Numerical Model for Depth-averaged Incompressible Flow', *Tech. Rep. REMR-HY-11*, U.S. Army Engineer Waterways Experiment Station, Vicksburg, Miss.

Bradbrook, K. F., Biron, P. M., Lane, S. N., Richards, K. S. and Roy, A. G.: 1998, 'Investigation of controls on secondary circulation and mixing processes in a simple confluence geometry using a three-dimensional numerical model', *Hydrol. Process.* **12**, 1371–1396.

Bradbrook, K. F., Lane, S. N. and Richards, K. S.: 2000, 'Numerical simulation of three-dimensional, time-averaged flow structure at river channel confluences', *Water Resour. Res.* **36**(9), 2731–2746.

Bombardelli, F. A., Hirt, C. W. and García, M. H.: 2001, 'Discussion on 'Computations of Curve Free Surface Water Flow on Spiral Concentrators' ' by B. W. Matthews, C. A. J. Fletcher, A. C. Partridge and S. Vasquez, *J. Hydr. Eng. ASCE* **127**(7), 629–630.

Chow, V. T.: 1959, *Open Channel Hydraulics*, McGraw-Hill.

Crowder, D. W. and Diplas, P.: 2000, 'Using two-dimensional hydrodynamic models at scales of ecological importance', *J. Hydrology* **230**, 172–191.

Dietrich, W. E.: 1987, 'Mechanics of Flow and Sediment Transport in River Bends', in Richards (ed.), *River Channels: Environment and Process*, Basil Blackwell Scientific Publications.

Finnie, J., Donnell, B., Letter, J. and Bernard, R.: 1993, 'Secondary flow correction for depth-averaged flow calculations', *J. Eng. Mech., ASCE* **125**(7), 109–124.

Frothingham, K. M.: 2001, 'Geomorphological Processes in Meandering and Straight Reaches of an Agricultural Stream in East Central Illinois: Relations to Aquatic Habitat', *Ph.D. Thesis*, Geography Department, University of Illinois at Urbana-Champaign.

Frothingham, K. M., Rhoads, B. L. and Herricks, E. E.: 2002, 'A multiscale conceptual framework for integrated ecogeomorphological research to support stream naturalization in the agricultural Midwest', *Environ. Manage.* **29**(1), 16–33.

Frothingham, K. M., Rhoads, B. L. and Herricks, E. E.: 2001, 'Stream Geomorphology and Fish Community Structure in Channelized and Meandering Reaches of an Agricultural Stream', in J. Dorava, D. Montgomery, B. Palscak and F. Fitzpatrick (eds), *Geomorphic Processes and Reverine Habitat*, American Geophysical Union, Washington, DC.

García, M. H., Bittner, L. and Niño, Y.: 1994, 'Mathematical Modeling Meandering Streams in Illinois: A Tool for Stream Management and Engineering', *Civil Engineering Studies, Hydraulic Eng. Series No. 43*, University of Illinois at Urbana-Champaign.

Hirt, C. W. and Nichols, B. D.: 1981, 'Volume of Fluid (VOF) method for the dynamics of free boundaries', *J. Comp. Physics* **39**, 201–225.

Hirt, C. W. and Sicilian, J. M.: 1985, 'A Porosity Technique for the Definition of Obstacles in Rectangular Cell Meshes', *Proc. Fourth Int. Conf. Ship Hydro.*, National Academy of Science, Washington, DC.

Hodkinson, A. and Ferguson, R. I.: 1998, 'Numerical modeling of separated flow in river bends: Model testing and experimental investigation of geometric controls on the extent of the flow separation on the concave bank', *Hydrol. Process.* **12**, 1323–1338.

Ikeda, S., Parker, G. and Sawai, K.: 1981, 'Bend theory of river meanders', *J. Fluid Mech.* **112**, 363–377.

Johannesson, H. and Parker, G.: 1989, 'Linear Theory of River Meanders', in Ikeda and Parker (eds), *River Meandering*, Water Resources Monograph, AGU.

Lane, S., Richards, K. and Chandler, J.: 1995, 'Within-reach Spatial Patterns of Process and Channel Adjustment', in Hickin (ed.), *River Geomorphology*, John Wiley & Sons Ltd.

Lane, S., Bradbrook, K., Richards, K., Biron, P. and Roy, A.: 1999, 'The application of computational fluid dynamics to natural river channels: Three-dimensional versus two-dimensional approaches', *Geomorphology* **29**, 1–20.

Leschziner, M. and Rodi, W.: 1979, 'Calculation of strongly curved open channel flow', *J. Hydraul. Eng. ASCE* **105**, 1297–1314.

López, F.: 1997, 'Open-channel Flow with Roughness Elements of Different Spanwise Aspect Ratios: Turbulence Structure and Numerical Modeling', *Ph.D. Thesis*, Department of Civil and Environmental Engineering, University of Illinois at Urbana-Champaign.

Naot, D., Nezu, I. and Nakagawa, H.: 1993, 'Hydrodynamic behavior of compound rectangular open channels', *J. Hydraul. Eng. ASCE* **119**, 390–408.

Nelson, J. and Smith, D.: 1989, 'Flow in Meandering Channels with Natural Topography', in Ikeda and Parker (eds), *River Meandering*, Water Resources Monograph, AGU.

Nicholas, A. P.: 2001, 'Computational fluid dynamics modeling of boundary roughness in gravel-bed rivers: An investigation of the effects of random variability in bed elevation', *Earth Surf. Process. Landforms* **26**, 345–362.

Olsen, N. R. B. and Stokseth, S.: 1995, 'Three-dimensional numerical modelling of water flow in a river with large bed roughness', *J. Hydr. Res.* **33**(4), 571–581.

Rhoads, B. L. and Welford, M. R.: 1991, 'Initiation of river meandering', *Progr. Phys. Geogr.* **15**, 127–156.

Rhoads, B. L. and Sukhodolov, A.: 2001, 'Field investigation of three-dimensional flow structure at stream confluences: 1. Thermal mixing and time-averaged velocities', *Water Resour. Res.* **37**(9), 2393–2410.

Rodi, W.: 1984, *Turbulence Models and their Application in Hydraulics*, IAHR Monograph, Delft.

Sukhodolov, A. and Rhoads, B. L.: 2001, 'Field investigation of three-dimensional flow structure at stream confluences: 2. Turbulence', *Water Resour. Res.* **37**(9), 2411–2424.

Weerakoon, S. B. and Tamai, N.: 1989, 'Three-dimensional calculation of flow in river confluences using boundary fitted coordinates', *J. Hydrosci. Hydraul. Eng.* **7**, 51–62.

Wu, W., Rodi, W. and Wenka, T.: 1997, 'Three-dimensional Calculation of River Flow', *Proc. 27th IAHR Congress*, San Francisco, CA.

Yen, C. and Yen, B. C.: 1971, 'Water surface configuration in channel bends', *J. Hydraul. Div. ASCE* **97**(HY2), 303–321.